

Annual Review of Pharmacology and Toxicology
Structure and Pharmacology
of Voltage-Gated Sodium
and Calcium Channels

William A. Catterall, Michael J. Lenaeus,
and Tamer M. Gamal El-Din

Department of Pharmacology and Division of General Internal Medicine, Department of
Medicine, University of Washington, Seattle, Washington 98195, USA; email: wcatt@uw.edu

Annu. Rev. Pharmacol. Toxicol. 2020. 60:133–54

First published as a Review in Advance on
September 19, 2019

The *Annual Review of Pharmacology and Toxicology* is
online at pharmtox.annualreviews.org

<https://doi.org/10.1146/annurev-pharmtox-010818-021757>

Copyright © 2020 by Annual Reviews.
All rights reserved

Keywords

sodium channels, calcium channels, local anesthetics, antiarrhythmic drugs, calcium antagonist drugs

Abstract

Voltage-gated sodium and calcium channels are evolutionarily related transmembrane signaling proteins that initiate action potentials, neurotransmission, excitation-contraction coupling, and other physiological processes. Genetic or acquired dysfunction of these proteins causes numerous diseases, termed channelopathies, and sodium and calcium channels are the molecular targets for several major classes of drugs. Recent advances in the structural biology of these proteins using X-ray crystallography and cryo-electron microscopy have given new insights into the molecular basis for their function and pharmacology. Here we review this recent literature and integrate findings on sodium and calcium channels to reveal the structural basis for their voltage-dependent activation, fast and slow inactivation, ion conductance and selectivity, and complex pharmacology at the atomic level. We conclude with the theme that new understanding of the diseases and therapeutics of these channels will be derived from application of the emerging structural principles from these recent structural analyses.

ANNUAL
REVIEWS **CONNECT**

www.annualreviews.org

- Download figures
- Navigate cited references
- Keyword search
- Explore related articles
- Share via email or social media

1. INTRODUCTION

Voltage-gated sodium (Na_V) channels initiate and conduct action potentials in nerve, muscle, and other electrically excitable cells (1). The basic functional properties of sodium and calcium channels were elucidated in classical electrophysiological studies using the voltage clamp method. Upon depolarization of nerve or muscle fibers, Na_V channels are rapidly activated and initiate the action potential (2). Within a few milliseconds, sodium channels undergo fast inactivation, which returns the sodium conductance through them nearly to the baseline level (2). Prolonged depolarization or repetitive depolarizations drive sodium channels into a distinct slow-inactivated state from which recovery is very slow (3, 4). Sodium conductance is mediated by an ion selectivity filter that catalyzes sodium entry and restricts the passage of other ions (5, 6). Na_V channels are subject to regulation by intracellular signaling pathways, and they are the molecular targets for neurologic, psychiatric, and cardiovascular diseases and for related therapeutic agents (7, 8). Calcium currents were first recorded in cardiac muscle, where depolarization activates voltage-gated channels that are highly selective for calcium (9, 10). Voltage-gated calcium (Ca_V) channels are activated during action potentials in many types of excitable cells, and they conduct calcium into cells to initiate numerous physiological processes, including contraction, neurotransmission, secretion, and gene transcription (1, 11). Classical calcium channel–blocking drugs are used in the treatment of cardiovascular disorders, including cardiac arrhythmia, hypertension, and angina pectoris (12, 13).

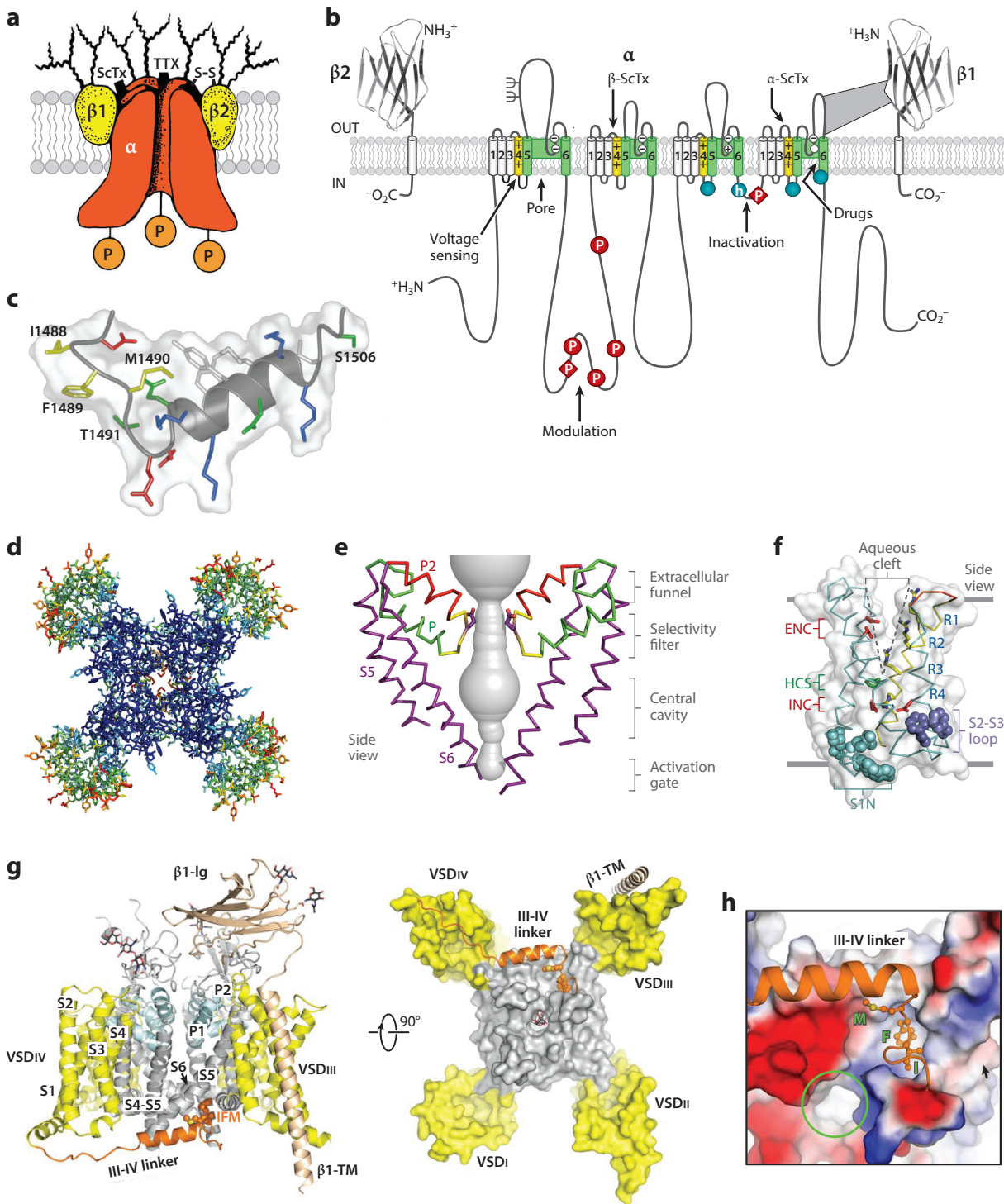
Recent work has given new atomic-level insights into the structure and function of sodium and calcium channels as well as the sites and mechanisms of action of therapeutic agents that act on them. Na_V and Ca_V channels are closely related members of the voltage-gated ion channel protein superfamily, sometimes referred to as the chanome (14; <http://www.guidetopharmacology.org/GRAC/ReceptorFamiliesForward?type=IC>). Their close molecular relationships derive from their common ancestor, the bacterial sodium channels related to NaChBac (14, 15). Here we review the structure, function, and pharmacology of these kissing-cousin ion channels, which are about 25% identical in amino acid sequence in their conserved transmembrane domains.

2. STRUCTURE AND FUNCTION OF SODIUM AND CALCIUM CHANNELS

2.1. Purification and Subunit Structure

Sodium channel proteins isolated from nerve and muscle based on high-affinity neurotoxin binding are complexes of a large, pore-forming α subunit of 250 kDa with one or two β subunits of 30–40 kDa (7, 16) (**Figure 1a**). The α subunits are composed of 24 transmembrane segments organized in four homologous domains containing six transmembrane segments in each (7, 16–18) (**Figure 1b,c**). In contrast, the $\text{Na}_V\beta$ subunits are single membrane-spanning glycoproteins with a small intracellular domain and an extracellular immunoglobulin-like domain, similar to cell adhesion molecules (7, 19, 20) (**Figure 1b**). Expression of the α subunit alone is sufficient to reconstitute sodium channel function in *Xenopus* oocytes or mammalian cells, but the β subunits modify the kinetics and voltage dependence of sodium channel activation and inactivation (7, 19, 20).

Ca_V channels were initially purified, reconstituted, and cloned from skeletal muscle, where they play a key role in excitation-contraction coupling (21–23). They were isolated based on high-affinity binding of dihydropyridine calcium antagonist drugs. Calcium channels have a central pore-forming subunit, designated $\alpha 1$, which has a transmembrane folding pattern like the α subunit of sodium channels (11, 22, 24) (**Figure 1b**). This pore-forming subunit is associated with



(Caption appears on following page)

Figure 1 (Figure appears on preceding page)

Structural components of Na_V channels. (a) Representation of a brain sodium channel based on biochemical studies. Wavy lines depict N-linked glycosylation. (b) Transmembrane folding diagram of the sodium channel subunits, with the extracellular domains of the β subunits represented as immunoglobulin-like folds. Blue circles indicate fast inactivation gate receptor components. (c) Structure of the fast inactivation gate in solution as determined by nuclear magnetic resonance. (d) Structure of the bacterial sodium channel Na_VAb viewed from the extracellular side, including the pore module (dark blue) and the voltage sensor (green and red). (e) Pore domain of Na_VAb viewed from the membrane perspective. Only the pore-forming S5, P, P2, and S6 segments of two subunits are shown, with gray indicating water-accessible space in the pore. (f) Voltage sensor of Na_VAb . (g) Structure of the human $\text{Na}_V1.4$ channel. (h) Inactivation gate of $\text{Na}_V1.4$ channels. The IFM forms the fast inactivation particle in the linker connecting domains III and IV. Abbreviations: ENC, extracellular negative cluster; h, fast inactivation particle; HCS, hydrophobic constriction site; IFM, isoleucine-phenylalanine-methionine motif; Ig, immunoglobulin-like; INC, intracellular negative cluster; Na_V , voltage-gated sodium; P, sites of protein phosphorylation; -S-S-, disulfide bond; S1N, N-terminal alpha helix preceding transmembrane segment S1; ScTx, scorpion toxin; TM, transmembrane; TTX, tetrodotoxin; VSD, voltage-sensing domain. Panels a–c adapted with permission from Reference 7; panels d–f adapted with permission from Reference 25; and panels g,h adapted with permission from Reference 32.

up to four distinct classes of auxiliary subunits: an intracellular β subunit; a membrane-associated, disulfide-linked $\alpha\delta$ subunit complex; and a transmembrane γ subunit (11, 21, 24) (**Figure 2a**). A preprotein containing α 2 and δ subunits is encoded by a single gene, and the mature subunits are produced by proteolytic processing at two sites, disulfide linkage, and the addition of a C-terminal glycoposphatidylinositol anchor (11, 20, 24). These four classes of auxiliary subunits modify calcium channel gating as well as assembly and insertion into the plasma membrane (11, 20, 24).

2.2. The Transmembrane Core of Sodium and Calcium Channels

The three-dimensional structure of the core functional unit of the sodium channel was first revealed by X-ray crystallographic studies of the homotetrameric ancestral bacterial sodium channel (Na_VAb) (25) (**Figure 1d**). As expected from structures of potassium channels, the pore is formed by the S5 and S6 segments in the center of a square array of four subunits, and the voltage sensor is formed by a bundle of four transmembrane alpha-helices (S1–S4) connected to the pore by the S4–S5 linker (8, 25, 26) (**Figure 1b**). Structure-function studies using mutagenesis, electrophysiology, and molecular modeling have given a detailed two-dimensional map of the functional parts of sodium channels (7, 8, 26) (**Figure 1b**). Voltage-dependent activation is initiated by voltage-driven outward movement of the positive gating charges, usually arginine residues, in the S4 transmembrane segments of the voltage sensors (7, 27–29) (**Figure 1b,f**). Sodium conductance is mediated by the pore domain formed by the S5 and S6 segments and the P loop between them (7, 8, 26) (**Figure 1b,e**). Within 1–2 ms after opening, the fast inactivation gate formed by the intracellular linker connecting domains III and IV folds into the pore and inactivates it (7, 8, 26) (**Figure 1b,c**). During prolonged depolarization, sodium channels enter a slow-inactivated state from which recovery requires prolonged repolarization (30, 31).

2.3. The Eukaryotic Sodium and Calcium Channel Complexes

Cryo-electron microscopic (cryoEM) analysis of eukaryotic nerve and skeletal muscle sodium channel complexes has given dramatic new insights into their overall structure (32–35) (**Figure 1g,b**). The structure of the functional cores of these channels is virtually identical to Na_VAb (25), which was used as a search template to solve the initial structure (34). The backbones of the pores and ion selectivity filters in the center of these structures are essentially identical to their bacterial ancestors, but the high field-strength site in vertebrate sodium channels has four different side chains: Asp-Glu-Lys-Ala (32–35). The voltage sensors are in a similar activated conformation to that observed for bacterial Na_V channels (32–34) (**Figure 1f**). In addition to these

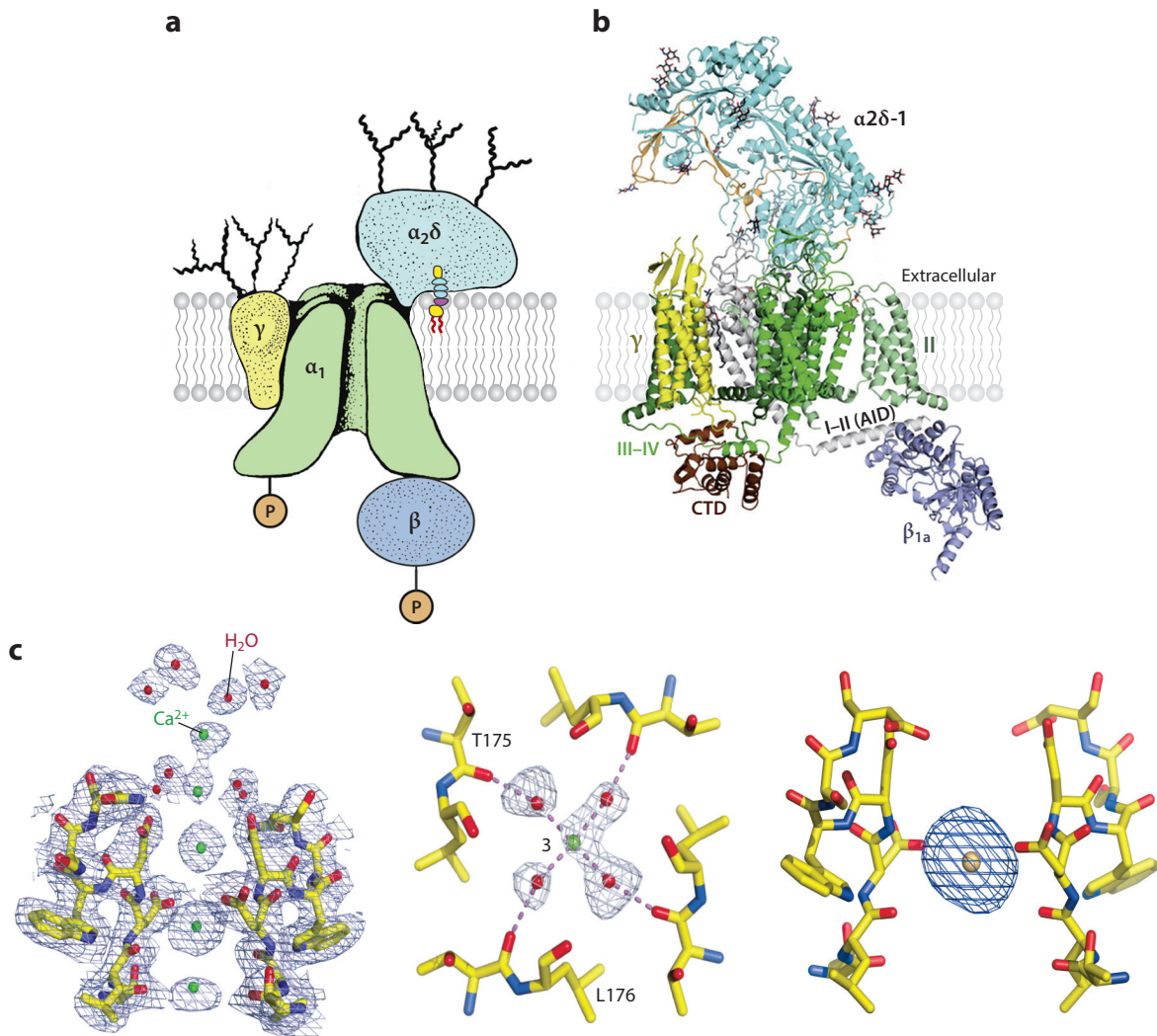


Figure 2

Structural components of Cav channels. (a) Representation of the skeletal muscle calcium channel based on biochemical studies. Panel a adapted with permission from Reference 156. (b) Structure of the skeletal muscle $\text{Cav}1.1$ channel determined by cryo-electron microscopy. Panel b adapted with permission from References 37 and 156. (c) Structure of the ion selectivity filter of CavAb . (Left) The selectivity filter of CavAb with a line of Ca^{2+} ions (green) and immobilized water molecules (red). The narrow point in the selectivity filter is the high field-strength site formed by Asp177. (Center) A Ca^{2+} ion with surrounding waters of hydration bound at site 3, which is formed by the backbone carbonyls of Thr175. (Right) A single blocking Cd^{2+} ion bound to Asp177 in the high field-strength site. Electron density is illustrated by the mesh. Panel c adapted with permission from Reference 58. Abbreviations: AID, α interaction domain; Cav , voltage-gated calcium; CavAb , ancestral bacterial calcium channel construct.

new insights into the core functional unit of sodium channels, the cryoEM studies of eukaryotic sodium channels have generated extraordinary new information on the structure of the complex of α and β subunits, the conformation of the fast inactivation gate in situ, and the partial structures of the large intracellular and extracellular domains that are not present in the bacterial Nav channels (32–35) (Figure 1g,b).

The first structure of a eukaryotic calcium channel was determined for the Cav1.1 channel purified from rabbit skeletal muscle, using biochemical methods similar to those employed originally for isolation of the channel protein (21, 36, 37) (**Figure 2a,b**). This structure elegantly confirms the overall subunit composition and structure of the calcium channel determined with biochemical methods and gives much more detail on the conformation of the five subunits (36, 37) (**Figure 2a,b**). As expected from previous crystallographic studies (38, 39), the β subunit contains an SH3 domain that may interact with other cellular proteins and an NK domain that interacts with the intracellular linker connecting domains I and II of the α_1 subunit through the α interaction domain (37). The heavily glycosylated α_2 subunit projects far into the extracellular space, consistent with its postulated role as a cell adhesion molecule (24). Only the extracellular portion of the full-length $\alpha_2\delta$ precursor protein is observed in the cryoEM structure, consistent with biochemical studies showing that the C-terminal region of the δ subunit is proteolytically processed and linked to the membrane by a glycosylphosphatidylinositol anchor (40).

2.4. Voltage-Dependent Activation

The voltage-dependent activation of sodium channels is driven by transmembrane movement of the Arg gating charges in the S4 segments of the voltage sensors. Classical studies detected this transmembrane charge movement as an outward capacitive gating current, whose magnitude is equivalent to movement of 2–3 gating charges across the transmembrane electrical field per voltage sensor (28, 41). The implied outward movement of the sodium channel S4 segment has been detected in voltage-dependent chemical labeling and disulfide-locking studies (42–46). The NavAb voltage sensor is a four-helix bundle with a substantial aqueous cleft that faces the extracellular milieu (25) (**Figure 1b,f**). The gating charges in the S4 segment are usually Arg residues spaced at three-residue intervals, which span the membrane (see R1–4 in **Figure 1f**). Upon depolarization, the S4 segment moves outward, exchanging ion pair partners and transporting the Arg gating charges through the hydrophobic constriction site (HCS) according to a sliding-helix model (44–48) (see HCS in **Figure 1f**). The presence of the large side chain of the Arg gating charges serves to seal the voltage sensor and prevent transmembrane movement of water and ions. Changes in membrane potential drive the S4 segment inward and outward in response to hyperpolarization and depolarization, moving the gating charges through the HCS and across the complete transmembrane electric field (47). These voltage-driven conformational changes provide electromechanical coupling of depolarization and repolarization to opening and closing of the pore, respectively.

Pore opening takes place at the intracellular ends of the S6 segments, which cross and interact closely to form the closed activation gate (**Figures 1e and 3a**) (25, 26, 49). The bundle of S6 helices opens in an iris-like motion in response to voltage-dependent conformational changes in the voltage sensor (25, 26, 49) (**Figure 3a**). Structures of the sodium channel in open states reveal a substantial movement of the intracellular ends of the S6 segments, from a closed conformation with an orifice of less than 1 Å to an open conformation with an orifice of up to 10.5 Å (50) (**Figure 3a**). This large opening is just sufficient to allow passage of hydrated sodium ions without a significant energy barrier (50). The open activation gate just fills the space between the surrounding S4–S5 segments, suggesting that this open conformation is as large as possible without major additional structural rearrangements.

In work completed after this review was submitted for publication, we determined the structure of NavAb in the resting state, giving the first insight into the structural basis for voltage-dependent activation of the voltage sensor and its coupling to opening the pore (51). The resting state is characterized by the inward movement of the S4 gating charges through the voltage sensor by

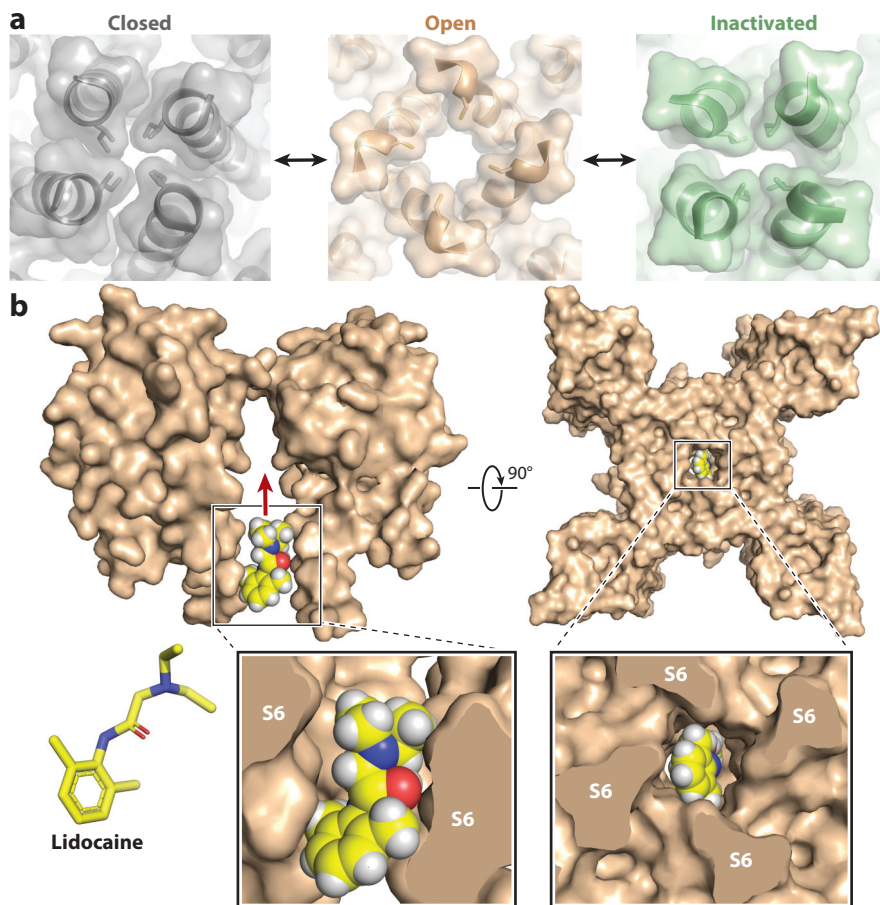


Figure 3

Open and closed states and lidocaine binding in the pore of the ancestral bacterial sodium channel (NavAb). (a) Closed, open, and inactivated states of the activation gate of NavAb in a space-filling model. The orifice in the activation gate is 10.5 Å. Panel *a* adapted with permission from Reference 50. (b, left) The open state of NavAb is shown in a space-filling model in wheat. Lidocaine entry through the open activation gate is shown in a side view, with lidocaine manually placed in the model for illustrative purposes. The inset shows a stick model of lidocaine (left) and a close-up of lidocaine's entry pathway (right). (b, right) Lidocaine moving through the open activation gate as viewed from the intracellular side of the membrane. The inset shows a close-up of lidocaine's entry pathway.

11.5 Å, the unwinding of the extracellular S3-S4 loop and the outer end of the S4 helical segment, and the formation of a characteristic elbow of the S4-S5 linker projecting into the cytoplasmic compartment (51). In this inward position, the voltage sensor in the resting state is poised to shoot outward upon depolarization and drive the opening of the pore. The voltage-dependent gating mechanism derived from this high-resolution structure agrees closely with the sliding helix model of voltage-dependent gating, as illustrated in the previous Rosetta model of gating based on the structure of the activated state of NavAb (25) (**Figure 1f**) and disulfide-locking studies (44–48). The complete voltage-dependent gating mechanism, from voltage sensing to pore opening, is now defined at the atomic level.

Because they are derived from a common ancestor, it is likely that Ca_V channels have similar voltage-dependent activation, conformational coupling, and pore-opening mechanisms to Na_V channels.

2.5. Sodium Conductance and Selectivity

As for voltage-gated potassium channels, sodium conductance and selectivity are mediated by the P loops in the four pore-forming modules of sodium channels (**Figure 1e**), which interact with Na^+ as it approaches and enters the ion selectivity filter (25, 52–55). However, in sharp contrast to potassium channels, the outward-facing edge of the ion selectivity filter is composed of a square array of four glutamate (Glu) residues in bacterial Na_V channels (25) or an array of four different amino acid residues, Asp-Glu-Lys-Ala, in metazoan Na_V channels (32). This high field-strength site partially dehydrates the approaching Na^+ ion and allows only Na^+ to pass efficiently (52–54). Unexpectedly, the side chains of the Glu residues at the high field-strength site move inward with each Na^+ by rotating at a single torsion angle in a dunking motion that takes place at the rate of Na^+ permeation, $> 10^7$ per second (52, 56). This dunking motion allows Na^+ to be conducted in a degenerate set of partially dehydrated complexes with the Glu side chains and increases the rate of Na^+ conductance.

2.6. Calcium Selectivity

Vertebrate Ca_V channels have an ion selectivity filter with a high field-strength site containing four Glu residues, similar to Na_VAb and the other bacterial sodium channels (24, 55). These residues are crucial for calcium selectivity and conductance in eukaryotic calcium channels (55). The addition of negatively charged residues in the outer vestibule of Na_VAb , following the pattern in eukaryotic calcium channels (57), converts Na_VAb to a form with high calcium selectivity, designated Ca_VAb (58). Determination of the structure of Ca_VAb by X-ray crystallography revealed a series of closely spaced Ca^{2+} binding sites at approximately 4-Å intersite intervals that lead through the ion selectivity filter (58) (**Figure 2c**). These sites are occupied sequentially by Ca^{2+} as it moves inward through the pore. Like Na^+ , Ca^{2+} is conducted as a hydrated cation, and waters of hydration can be resolved in favorable crystal structures (58) (**Figure 2c**). As originally proposed in biophysical models of Ca^{2+} permeation (59–61), these sites bind Ca^{2+} with high affinity in order to prevent monovalent cation permeation, and yet they give high conductance of Ca^{2+} by the knock-off effect of electrostatic repulsion of one entering Ca^{2+} on the preceding Ca^{2+} ions in the pore (58). Consistent with the requirement for a series of Ca^{2+} -binding sites for conductance, Cd^{2+} binds to a single site and blocks the pore but is not conducted (58) (**Figure 2c**).

2.7. Slow Voltage-Dependent Inactivation

In response to prolonged single depolarizations or trains of repetitive depolarizations, Na_V channels enter a distinct slow-inactivated state that is very stable (3, 4, 30, 62), and this process is modulated by neurotransmitter receptors and second messenger signaling pathways through protein phosphorylation (31). Recovery from slow inactivation requires prolonged repolarization. Slow voltage-dependent inactivation is characteristic of all sodium channels, from bacteria to human (30, 63–65). Slow inactivation of the bacterial sodium channels is caused by an asymmetric collapse of the pore, involving amino acid residues in the ion selectivity filter and the pore-lining S6 segments (26, 66–69). In eukaryotic sodium channels, this mechanism closes the pore on a longer time scale through conformational changes in the selectivity filter and the pore-lining S6 segment, and this form of inactivation is very slowly reversed upon repolarization (30, 70, 71).

Slow, voltage-dependent inactivation is also observed for Ca_V channels (72–74). This form of inactivation is observed most easily in experiments in which Ba^{2+} is substituted for Ca^{2+} as the permeant ion in order to prevent the more rapid Ca^{2+} /calmodulin-dependent inactivation that is characteristic of many calcium channels (75, 76). Disease mutations in amino acid residues at the intracellular ends of the S6 segments of $\text{Ca}_V1.2$ and $\text{Ca}_V1.3$ channels prevent slow, voltage-dependent inactivation (77–81). These results are consistent with an asymmetric collapse of the S6 segments during this form of Ca_V channel inactivation, as observed for bacterial Na_V channels (66, 67). Slow, voltage-dependent inactivation of sodium and calcium channels is also an important allosteric modulator of drug binding and block, as described below (82–84).

2.8. Fast Voltage-Dependent Inactivation

Fast inactivation is a crucial evolutionary addition to basic sodium channel function, as it is observed in eukaryotic sodium channels but not in prokaryotic sodium channels (63, 85). The fast inactivation gate of the eukaryotic sodium channels is formed by the intracellular linker between domains III and IV (86–89), which is not present in the structure of bacterial sodium channels (**Figure 1b,d**). A series of key amino acid residues in the intracellular linker connecting domains III and IV, Ile-Phe-Met-Thr, serve as the classically defined inactivation particle, which folds into the inner mouth of the pore and blocks sodium conductance (89) (**Figure 1c**). The structure of the fast inactivation gate peptide analyzed as a separate protein in solution by nuclear magnetic resonance contains an alpha-helical motif preceded by two turns containing the key interacting residues in the Ile-Phe-Met-Thr motif (90) (**Figure 1c**). During fast inactivation, these key amino acid residues are projected into the intracellular mouth of the pore, where they are bound and block ion permeation (32, 90). Remarkably, the structure of the fast inactivation gate peptide determined in solution is very similar to its conformation in the full-length $\text{Na}_V1.4$ channel (32, 90) (**Figure 1g,b**). The receptor that binds the inactivation gate to the intracellular end of the pore is formed by amino acid residues in the S4-S5 linkers in domains III and IV and in the intracellular end of the S6 segment in domain IV (32, 33, 91–95) (**Figure 1b,b**). Structure-function studies showed that scorpion toxins block fast inactivation by binding to the S3-S4 linker and preventing the outward movement of the gating charges in domain IV (96, 97). Similarly, studies using fluorescent labeling of S4 segments and voltage-clamp fluorometry revealed that the outward movement of the gating charges in the S4 segment of the voltage sensor in domain IV plays a key role in coupling activation to fast inactivation (98, 99).

3. SODIUM AND CALCIUM CHANNEL PHARMACOLOGY AT THE ATOMIC LEVEL

3.1. State-Dependent Drug Block

Voltage-gated sodium channels are the molecular targets for drugs used in local anesthesia and in the treatment of epilepsy, chronic pain, and cardiac arrhythmia (1, 82, 100, 101). All of these drugs block Na_V channels in a state-dependent manner, depending on the resting membrane potential and the frequency of action potential generation (1, 82, 100, 101). Voltage-dependent block increases the inhibition of sodium currents in depolarized cells that are damaged and driving inappropriate action potential generation. Frequency-dependent block increases inhibition of sodium currents in rapidly firing cells that transmit pain information and drive hyperexcitability in epilepsy and cardiac arrhythmia. This state-dependent action is essential to allow the drugs to preferentially block sodium channels in depolarized, rapidly firing cells that cause pain, epilepsy,

and cardiac arrhythmia without blocking normal action potential generation in sensory nerves, brain, or heart.

Classical calcium channel blockers are primarily used in the treatment of cardiovascular disorders (12, 13). They are grouped in three chemical classes, which have distinct functional effects and clinical uses (12, 13). Phenylalkylamines and benzothiazepines are primarily used for cardiac arrhythmia (102). They have strongly frequency-dependent block, which enhances their action on calcium channels in rapidly firing injured cardiac myocytes that are responsible for arrhythmia relative to uninjured myocytes contracting at a normal rate (82). Dihydropyridines are primarily used for hypertension and angina pectoris (12). They have strongly voltage-dependent block, which is driven by high-affinity binding to voltage-dependent calcium channels in the inactivated state (103). They preferentially inhibit calcium channels in continuously depolarized cells, such as the vascular smooth muscle cells that sustain contraction of blood vessels in hypertension and angina pectoris (12). As for sodium channel blockers, state-dependent binding and action are essential for the clinical use of these calcium antagonist drugs.

State-dependent block of sodium channels by local anesthetic and antiarrhythmic drugs is well described by the classical Modulated Receptor Hypothesis (1, 100, 104, 105). In this model, drug block is frequency-dependent because the receptor site is located in the pore and is more rapidly accessible for drug binding when the pore is open; therefore, the generation of action potentials at high frequency increases drug block (100). Drug block is voltage-dependent because these drugs bind to the inactivated state of sodium channels with high affinity; therefore, sodium channels in damaged, depolarized cells are preferentially blocked (100). Together, these mechanisms allow local anesthetics, antiepileptics, antiarrhythmics, and analgesics to have beneficial therapeutic effects without unwanted toxicity from complete block of electrical excitability (101).

Drug size, shape, and chemistry strongly influence modulated drug block (106, 107). Small, hydrophobic drug molecules can block sodium channels in the resting state, and it was hypothesized that these drugs can reach their receptor site in the pore by direct entry from the lipid phase of the membrane without pore opening (100, 107). These drugs are all secondary or tertiary amines with protonatable amino groups. The protonated, positively charged forms are the pharmacologically active molecular species of these drugs, as judged from experiments with variations in pH and with permanently charged local anesthetic derivatives (106, 108–110). Uncharged forms of these drugs diffuse across the cell membrane, are reprotonated in the cytosol, and block sodium channels from the inside of the cell. Damaged cells and tissues are often acidic; therefore, the pH of cells and tissues and the pKa values of the drugs modulate drug block in a complex way (106, 108, 109, 111).

Calcium antagonist drugs also conform to the general paradigm introduced in the Modulated Receptor Hypothesis (82, 83, 103). Frequency-dependent block by phenylalkylamines and benzothiazepines was proposed to result from binding in the pore, which is opened during each action potential and provides rapid drug access to their receptor site(s) (83). Voltage-dependent block by dihydropyridines was proposed to result from preferential binding to the inactivated conformation of calcium channels (103). Together, the frequency dependence and voltage dependence of drug action determine the clinical uses of these calcium antagonist drugs for cardiac arrhythmia versus hypertension and angina pectoris (82).

3.2. Drug Receptor Sites and the Structural Basis for State-Dependent Block of Sodium Channels

The initial molecular mapping studies of the receptor site for local anesthetic, antiepileptic, and antiarrhythmic drugs by site-directed mutagenesis revealed key amino acid residues in the

pore-lining S6 segment in domain IV, consistent with the model that these drugs enter and block the pore (112, 113). More detailed molecular mapping studies showed that amino acid residues in the IS6, IIIS6, and IVS6 segments converge to form the drug receptor site (114–118). Recent structural studies of NavAb with the drugs lidocaine and flecainide bound have further elucidated the three-dimensional structure of this important drug receptor site (119) (Figure 4*a,b*). The

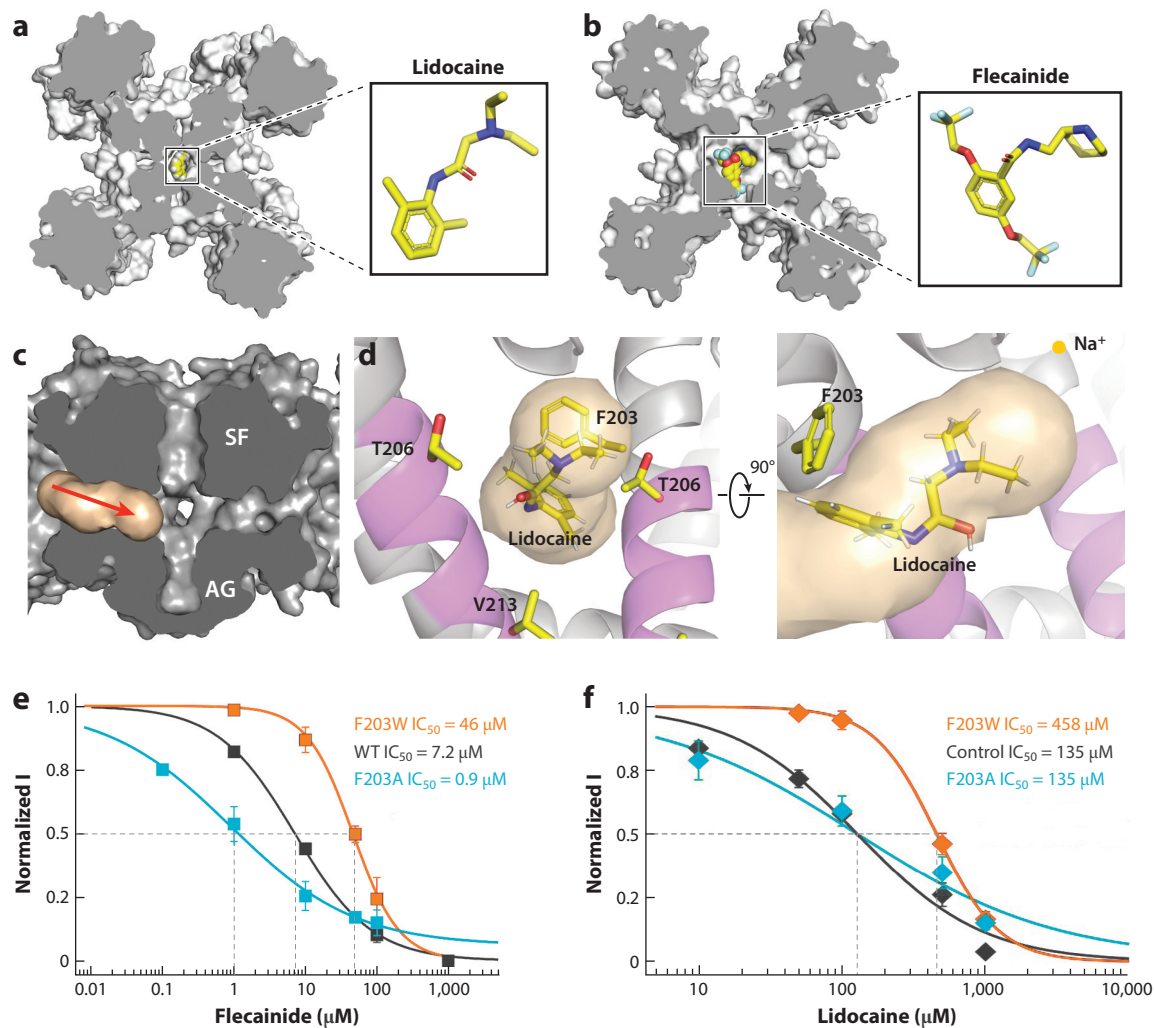


Figure 4

Drug receptor site and entry through the fenestrations of NavAb. (a) Intracellular view of lidocaine bound in its receptor site in the pore. (b) Intracellular view of flecainide bound in the pore. (c) A fenestration in NavAb viewed from the side in a section through the center of NavAb. Water-accessible space is indicated by the algorithm HOLE (*tan*), and the direction of drug entry is indicated (*red arrow*). (d) Lidocaine entry via the fenestrations. The water-accessible space in a fenestration indicated by the HOLE algorithm is illustrated in *tan*. The capping residue Phe203 and lidocaine are indicated in yellow sticks. (*Left*) Drug entry is viewed from the central cavity. (*Right*) Drug entry is viewed from the neighboring NavAb subunit as the drug moves from left to right into the central cavity of the pore. The sizes of the fenestrations and drug molecules are illustrated in accurate molecular scale. (e) Potency for flecainide block of NavAb (*black*), NavAb/F203A (*cyan*), and NavAb/F203W (*red*). (f) Potency for lidocaine block of NavAb (*black*), NavAb/F203A (*cyan*), and NavAb/F203W (*red*). Panels *e,f* adapted with permission from Reference 119. Abbreviations: AG, activation gate; NavAb, ancestral bacterial sodium channel; SF, selectivity filter.

electron density for bound lidocaine is located in the central cavity, just at the intracellular outlet of the narrow ion selectivity filter (119) (**Figure 4a,b**). A drug molecule bound in this position would completely block the ion permeation pathway. The essential protonated amino groups of lidocaine and flecainide point upward into the ion selectivity filter, where they interact with the backbone carbonyl groups of Thr175 that form the final coordination site for entering sodium ions in the selectivity filter of Na_VAb (119). Although flecainide binds in a similar position to lidocaine, it is larger and stretches further toward the walls of the central cavity (119) (**Figure 4b**).

What is the structural basis for modulated drug entry to the receptor site in the pore of sodium channels? Crystal structures of the open state of bacterial Na_V channels reveal an orifice at the activation gate of up to 10.5 Å in diameter (50) (**Figure 3a**). As illustrated in **Figure 3b**, an orifice of 10.5 Å is just sufficient to allow entry of lidocaine (50). Therefore, it is likely that the open activation gate provides the entry pathway for frequency-dependent block by these drugs. Although frequency-dependent block of Na_V channels can be measured directly by repetitively opening the pore, the proposed model of resting-state block by direct entry into the pore from the lipid phase of the membrane (100) has lacked experimental support. Remarkably, the crystal structure of Na_VAb revealed fenestrations in the side of the pore that lead from the lipid phase of the membrane into the central cavity at the position of the drug receptor site (25, 119) (**Figure 4c**). These fenestrations are conserved in eukaryotic Na_V channels (32–34), and they are large enough to allow passage of local anesthetic and antiarrhythmic drugs (119) (**Figure 4d**). Recent studies show that these fenestrations do indeed control block of Na_V channels in the resting state (119). Mutations of a key Phe residue (F203) that caps the fenestrations in Na_VAb change the size of the fenestrations without having an effect on the backbone conformation of the pore module (119). These mutations have large graded effects (up to 50-fold) on resting-state block by local anesthetics and antiarrhythmics that depend, predictably, on drug size (119). For example, these mutations shift the IC_{50} of flecainide, a large drug molecule, up to 50-fold (**Figure 4e**). In contrast, the IC_{50} for the smaller drug lidocaine is increased by the mutation F203W, which reduces the size of the fenestration, but is not affected by the mutation F203A, which increases the size of the fenestration, because lidocaine can already fit easily through the wild-type fenestration with F203 (**Figure 4f**). Thus, penetration through the fenestrations is a crucial determinant of the potency of state-dependent drug block. In the future, structure-based drug design should take account of the effects of fenestrations on drug access as well as the direct binding interactions of these pore-blocking drugs with their receptor site in the central cavity.

3.3. Drug Receptor Sites on Calcium Channels

Classical ligand-binding studies showed that the three chemical classes of calcium antagonist drugs interact with three partially overlapping, allosterically coupled receptor sites (120–122). Photoaffinity labeling identified the S6 segments in domains III and IV as the primary sites of drug interactions (123–128). These studies led to a model in which phenylalkylamines bind on the pore-facing side of the S6 segments and dihydropyridines bind to the lipid-facing side of the S6 segments (126). This general model has been confirmed by structural studies (discussed below).

More detailed molecular mapping by mutagenesis identified nine key amino acid residues in the IIIS5, IIS6, and IVS6 segments that form the dihydropyridine receptor site (129–133), and the transfer of these amino acid residues into dihydropyridine-insensitive calcium channels was sufficient to reconstitute dihydropyridine inhibition with nearly normal affinity and specificity (134–136). Similar molecular mapping studies identified an overlapping set of amino acid residues in the IIS6 and IVS6 plus amino acid residues in the ion selectivity filter that are important for binding of phenylalkylamines and benzothiazepines (137–142).

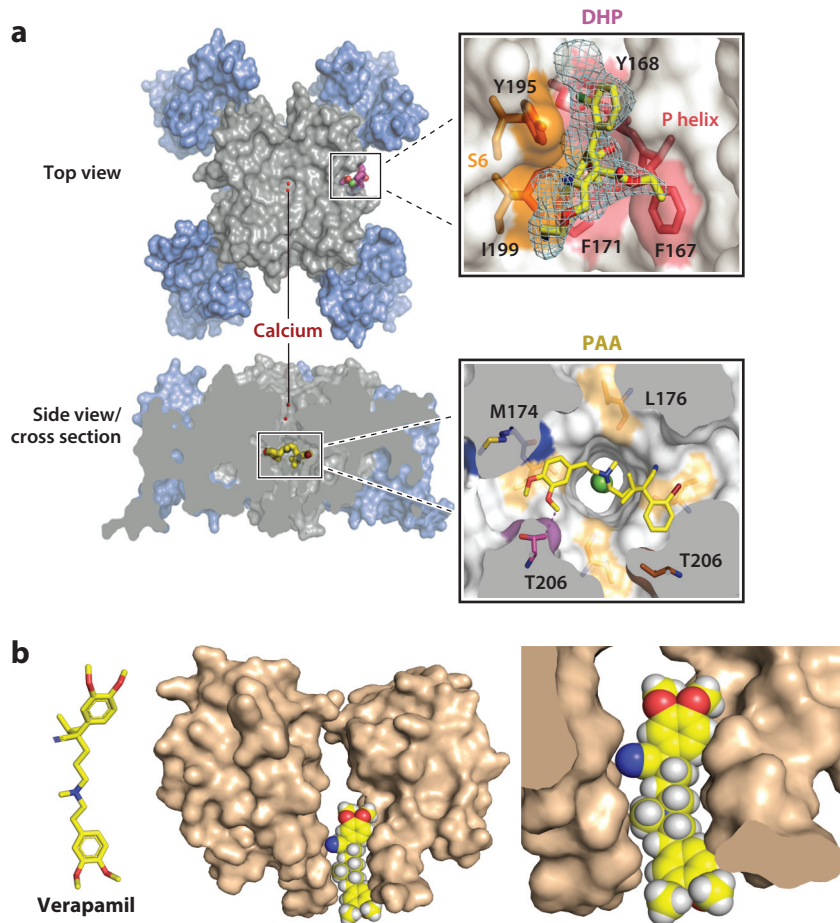


Figure 5

Receptor sites and pore entry for calcium antagonist drugs. (*a*) Calcium antagonist drugs at work. (*Top view*) Ca_vAb with the DHP amlodipine bound, calcium (*red*), the pore module (*gray*), and voltage sensors (*blue*). The inset shows the DHP amlodipine bound in its receptor site (DHP). Electron density is shown as a blue mesh, amlodipine as yellow sticks. (*Side view*) Cross section through Ca_vAb with the phenylalkylamine verapamil (*yellow sticks*) bound (PAA). The inset shows Ca²⁺ (*green*) and verapamil (*yellow sticks*). Panel *a* insets adapted with permission from Reference 143. (*b*) Verapamil entering the pore. Open-state structure of Ca_vAb with space-filling model of verapamil drawn to scale. Abbreviations: Ca_vAb, ancestral bacterial calcium channel; DHP, dihydropyridine; PAA, phenylalkylamine.

Surprisingly, Na_vAb and the calcium-selective derivative, Ca_vAb, have substantial binding affinity for calcium antagonist drugs, which leads to frequency- and voltage-dependent block at concentrations approximately tenfold higher than in mammalian cardiac calcium channels (15, 143). X-ray crystallography revealed two distinct receptor sites for phenylalkylamines and dihydropyridines in the model bacterial channel Ca_vAb (143) (**Figure 5a**). As expected, verapamil binds in the pore, just at the intracellular exit from the ion selectivity filter into the central cavity (143) (see PAA in **Figure 5a**). Its charged amino group projects upward into the pore, forming a complex with the backbone carbonyls of Thr175 at the intracellular end of the ion selectivity filter. Its two flanking aromatic moieties make hydrophobic interactions on either side of the

ion-conducting pathway through the ion selectivity filter, like the sticky ends of a Band-Aid (143) (**Figure 5a**). This binding pose for verapamil overlaps that of the sodium channel-blocking local anesthetic and antiarrhythmic drugs (50, 143) (**Figure 4a,b**), consistent with the model that frequency-dependent block by both sodium- and calcium-channel drugs results in a similar drug-receptor complex.

From electrophysiological studies, phenylalkylamines such as verapamil are thought to enter the pore and block it during single depolarizations (83, 144). These results are consistent with molecular mapping studies placing the receptor site on the pore-lining S6 segments in domains III and IV (137, 138). Like sodium channel-blocking drugs, verapamil is small enough in its extended conformation to enter the open activation gate (**Figure 5b**); however, larger drug molecules would be unable to enter. Thus, the size of the orifice formed by the open activation gate is an important determinant of open-channel, frequency-dependent block by calcium antagonist drugs.

In contrast to the phenylalkylamine receptor site, dihydropyridines such as amlodipine and nimodipine bind to a site on the external lipid-facing surface of the pore module between two voltage sensors (143) (see DHP in **Figure 5a**). Surprisingly, only a single dihydropyridine binds to the Ca_VAb homotetramer and induces a quaternary conformational change that prevents binding to the other three analogous positions in the tetrameric structure (143). This quaternary conformational change disrupts the fourfold symmetry of Ca_VAb and causes one Ca^{2+} to bind directly to a carboxyl side chain of an Asp residue in one of the coordination sites in the outer selectivity filter, effectively blocking the pore by tightly binding this Ca^{2+} ion. Thus, these structural findings indicate that the binding of dihydropyridines to a site on the lipid-facing surface of the pore module can effectively block Ca^{2+} conductance by inducing high-affinity binding of Ca^{2+} in the pore, as previously suggested from ligand-binding studies showing that binding of Ca^{2+} in the ion selectivity filter is required for high-affinity binding of dihydropyridines (129, 132). Recent X-ray crystallography studies indicate that the benzothiazepine diltiazem also binds in the pore of Ca_VAb in a position that partially overlaps the phenylalkylamine binding site (145). Therefore, frequency-dependent pore block by diltiazem and the allosteric interactions of diltiazem with dihydropyridines may involve the same molecular mechanisms as for verapamil and other phenylalkylamines.

After this review was submitted for publication, a new cryoEM structure of the skeletal muscle $\text{Ca}_V1.1$ channel appeared with calcium antagonist drugs bound (146). This work is a major addition to our understanding of the structural basis for calcium antagonist drug action. As previously described for the model calcium channel Ca_VAb , verapamil and diltiazem bound to overlapping receptor sites located in the central cavity of the pore on the intracellular side of the ion selectivity filter (146). In contrast, the receptor site for dihydropyridines was located on the lipid-facing surface of the pore module between the voltage sensors in domains III and IV (146), as expected from earlier structure-function studies of mammalian $\text{Ca}_V1.2$ channels (124–136) and from X-ray crystallography of Ca_VAb (143). These results add further crucial support for an indirect allosteric mechanism for pore block by dihydropyridines. As noted in previous studies of Ca_VAb , the dihydropyridine receptor site observed by X-ray crystallography was located about one to two helical turns toward the extracellular side of the channel from the amino acid residues expected to form that receptor site based on structure-function studies of mammalian $\text{Ca}_V1.2$ channels (145). The new structure of $\text{Ca}_V1.1$ with dihydropyridines bound resolves this apparent discrepancy by showing that dihydropyridines do indeed bind to the mammalian calcium channel in the position expected from the structure-function studies of mammalian $\text{Ca}_V1.2$ (146). Evidently, the dihydropyridines have their characteristic allosteric blocking effects on Ca_VAb by binding to a site that is adjacent to, but not exactly overlapping with, the dihydropyridine receptor site in mammalian calcium channels.

3.4. Drugs Acting on the Auxiliary Subunits of Sodium and Calcium Channels

Both sodium and calcium channels have auxiliary subunits that are required to fine-tune their functional properties and to support maturation and cell-surface expression of the channel complex (19, 20, 147, 148) (**Figures 1a,b** and **2a,b**). Only a single class of drugs, the gabapentinoid calcium channel antagonists gabapentin and pregabalin, act on the auxiliary subunits (147, 149). These drugs are used in therapy of epilepsy and chronic pain. They bind adjacent to a von Willebrand factor homology domain on the extracellular surface of the α_2 subunit and modulate the cell surface expression of $\text{Ca}_V2.2$ channels, which conduct N-type Ca^{2+} currents that are required for the release of neurotransmitters in the brain and in nociceptive pathways in the spinal cord (149). Drug binding disrupts normal recycling of these $\text{Ca}_V2.2$ channels to the cell surface and thereby reduces nociceptive signaling from the periphery to the central nervous system (150). Although the structure of the von Willebrand factor homology domain has been modeled based on its sequence homology, there are no direct structural studies of the binding and action of gabapentinoid drugs.

4. A FUTURE PERSPECTIVE ON SODIUM AND CALCIUM CHANNELS, DISEASE, AND THERAPEUTICS

Over the last few decades, many diseases have been attributed to mutations and other dysfunctions of Na_V and Ca_V channels. These channelopathies may result from a mutation in the encoding genes, or they may be acquired in the setting of tissue injury or autoimmune disease. To date, genetic variations in more than 60 ion channel genes have been correlated to human diseases (151, 152). In sodium channels alone, more than 1,000 disease-related mutations have already been identified (151). As a result, ion channels are considered one of the main targets of therapeutic medications, and 10–15% of drugs currently in the market target ion channels. Our understanding of how Na_V and Ca_V channels work has been elucidated in detail by the unprecedented advances in X-ray crystallography and cryoEM. We look forward to two important research thrusts resulting from this work. First, as illustrated by a recent study from our laboratory defining the structural basis for periodic paralysis (153), high-resolution structural studies will increasingly provide atomic-level views of disease processes and open new avenues for developing novel therapeutic approaches. This study revealed the binding pose of guanidinium in the mutant gating pore, which led to the idea that substituted guanidinium derivatives may block gating pore current without affecting the functionality of the voltage sensor in the skeletal muscle sodium channel (153, 154). Second, as illustrated here, we look forward to much more frequent use of high-resolution structural information in the development of medicines that target sodium and calcium channels with greater efficacy and safety. This experimental thrust is exemplified by the high-resolution structure analysis of the binding site of a new voltage-dependent inhibitor of $\text{Na}_V1.7$ channels that is under development for neuropathic pain (155). Structure-based design of more efficacious and safer treatments for chronic pain would be a huge benefit for patients and physicians and would provide an avenue leading out of the worldwide epidemic of opiate abuse.

DISCLOSURE STATEMENT

The authors are not aware of any affiliations, memberships, funding, or financial holdings that might be perceived as affecting the objectivity of this review.

ACKNOWLEDGMENTS

We acknowledge the deep insights and structural biology expertise provided by Dr. Ning Zheng (Professor of Pharmacology, University of Washington, and Investigator of the Howard Hughes Medical Institute) through his collaboration with us in all of our structural studies. Research from the authors' laboratories was supported by research grants from the National Institutes of Health to W.A.C. (R01 NS015751, R01 NS022625, and R01 NS025704) and to W.A.C. and Ning Zheng (R01 HL112808).

LITERATURE CITED

1. Hille B. 2001. *Ionic Channels of Excitable Membranes*. Sunderland, MA: Sinauer Associates Inc. 3rd ed.
2. Hodgkin AL, Huxley AF. 1952. A quantitative description of membrane current and its application to conduction and excitation in nerve. *J. Physiol.* 117:500–44
3. Adelman WJ, Palti Y. 1968. The effects of external potassium and long duration voltage conditioning on the amplitude of sodium currents in the giant axon of the squid *Loligo pealei*. *J. Gen. Physiol.* 54:589–606
4. Rudy B. 1978. Slow inactivation of the sodium conductance in squid giant axons. Pronase resistance. *J. Physiol.* 283:1–21
5. Hille B. 1972. The permeability of the sodium channel to metal cations in myelinated nerve. *J. Gen. Physiol.* 59:637–58
6. Hille B. 1975. Ionic selectivity, saturation, and block in sodium channels. A four-barrier model. *J. Gen. Physiol.* 66:535–60
7. Catterall WA. 2000. From ionic currents to molecular mechanisms: the structure and function of voltage-gated sodium channels. *Neuron* 26:13–25
8. Ahern CA, Payandeh J, Bosmans F, Chanda B. 2016. The hitchhiker's guide to the voltage-gated sodium channel galaxy. *J. Gen. Physiol.* 147:1–24
9. Reuter H. 1967. The dependence of slow inward current in Purkinje fibres on the extracellular calcium-concentration. *J. Physiol.* 192:479–92
10. Reuter H. 1983. Calcium channel modulation by neurotransmitters, enzymes and drugs. *Nature* 301:569–74
11. Catterall WA. 2011. Voltage-gated calcium channels. *Cold Spring Harb. Perspect. Biol.* 3:a003947
12. Godfraind T. 2017. Discovery and development of calcium channel blockers. *Front. Pharmacol.* 8:286
13. Fleckenstein A. 1983. History of calcium antagonists. *Circ. Res.* 52:13–16
14. Yu FH, Catterall WA. 2004. The VGL-chanome: a protein superfamily specialized for electrical signaling and ionic homeostasis. *Sci. STKE* 2004:re15
15. Ren D, Navarro B, Xu H, Yue L, Shi Q, Clapham DE. 2001. A prokaryotic voltage-gated sodium channel. *Science* 294:2372–75
16. Catterall WA. 1984. The molecular basis of neuronal excitability. *Science* 223:653–61
17. Noda M, Ikeda T, Kayano T, Suzuki H, Takeshima H, et al. 1986. Existence of distinct sodium channel messenger RNAs in rat brain. *Nature* 320:188–92
18. Trimmer JS, Cooperman SS, Tomiko SA, Zhou JY, Crean SM, et al. 1989. Primary structure and functional expression of a mammalian skeletal muscle sodium channel. *Neuron* 3:33–49
19. O'Malley HA, Isom LL. 2015. Sodium channel β subunits: emerging targets in channelopathies. *Annu. Rev. Physiol.* 77:481–504
20. Isom LL, De Jongh KS, Catterall WA. 1994. Auxiliary subunits of voltage-gated ion channels. *Neuron* 12:1183–94
21. Takahashi M, Seagar MJ, Jones JF, Reber BF, Catterall WA. 1987. Subunit structure of dihydropyridine-sensitive calcium channels from skeletal muscle. *PNAS* 84:5478–82
22. Tanabe T, Takeshima H, Mikami A, Flockerzi V, Takahashi H, et al. 1987. Primary structure of the receptor for calcium channel blockers from skeletal muscle. *Nature* 328:313–18
23. Leung AT, Imagawa T, Campbell KP. 1987. Structural characterization of the 1,4-dihydropyridine receptor of the voltage-dependent Ca^{2+} channel from rabbit skeletal muscle. Evidence for two distinct high molecular weight subunits. *J. Biol. Chem.* 262:7943–46

24. Zamponi GW, Striessnig J, Koschak A, Dolphin AC. 2015. The physiology, pathology, and pharmacology of voltage-gated calcium channels and their future therapeutic potential. *Pharmacol. Rev.* 67:821–70
25. Payandeh J, Scheuer T, Zheng N, Catterall WA. 2011. The crystal structure of a voltage-gated sodium channel. *Nature* 475:353–58
26. Catterall WA, Zheng N. 2015. Deciphering voltage-gated Na⁺ and Ca²⁺ channels by studying prokaryotic ancestors. *Trends Biochem. Sci.* 40:526–34
27. Catterall WA. 2010. Ion channel voltage sensors: structure, function, and pathophysiology. *Neuron* 67:915–28
28. Bezanilla F. 2000. The voltage sensor in voltage-dependent ion channels. *Physiol. Rev.* 80:555–92
29. Horn R. 2002. Molecular basis for function in sodium channels. *Novartis Found. Symp.* 241:21–26
30. Vilin YY, Ruben PC. 2001. Slow inactivation in voltage-gated sodium channels: molecular substrates and contributions to channelopathies. *Cell Biochem. Biophys.* 35:171–90
31. Cantrell AR, Catterall WA. 2001. Neuromodulation of Na⁺ channels: an unexpected form of cellular plasticity. *Nat. Rev. Neurosci.* 2:397–407
32. Pan X, Li Z, Zhou Q, Shen H, Wu K, et al. 2018. Structure of the human voltage-gated sodium channel Nav1.4 in complex with β 1. *Science* 362(6412):eaau2486
33. Shen H, Zhou Q, Pan X, Li Z, Wu J, Yan N. 2017. Structure of a eukaryotic voltage-gated sodium channel at near-atomic resolution. *Science* 335(6328):eaal4326
34. Yan Z, Zhou Q, Wang L, Wu J, Zhao Y, et al. 2017. Structure of the Nav1.4- β 1 complex from electric eel. *Cell* 170:470–82.e11
35. Pan X, Li Z, Huang X, Huang G, Gao S, et al. 2019. Molecular basis for pore blockade of human Na⁺ channel Nav1.2 by the μ -conotoxin KIIIA. *Science* 363:1309–13
36. Wu J, Yan Z, Li Z, Yan C, Lu S, et al. 2015. Structure of the voltage-gated calcium channel Cav1.1 complex. *Science* 350:aad2395
37. Wu J, Yan Z, Li Z, Qian X, Lu S, et al. 2016. Structure of the voltage-gated calcium channel Cav1.1 at 3.6 Å resolution. *Nature* 537:191–96
38. Van Petegem F, Clark KA, Chatelain FC, Minor DL Jr. 2004. Structure of a complex between a voltage-gated calcium channel β -subunit and an α -subunit domain. *Nature* 429:671–75
39. Chen YH, Li MH, Zhang Y, He LL, Yamada Y, et al. 2004. Structural basis of the α 1- β subunit interaction of voltage-gated Ca²⁺ channels. *Nature* 429:675–80
40. Davies A, Kadurin I, Alvarez-Laviada A, Douglas L, Nieto-Rostro M, et al. 2010. The α 28 subunits of voltage-gated calcium channels form GPI-anchored proteins, a posttranslational modification essential for function. *PNAS* 107:1654–659
41. Armstrong CM, Bezanilla F. 1973. Currents related to movement of the gating particles of the sodium channels. *Nature* 242:459–61
42. Yang N, George AL Jr., Horn R. 1996. Molecular basis of charge movement in voltage-gated sodium channels. *Neuron* 16:113–22
43. Yang N, Horn R. 1995. Evidence for voltage-dependent S4 movement in sodium channels. *Neuron* 15:213–18
44. DeCaen PG, Yarov-Yarovoy V, Zhao Y, Scheuer T, Catterall WA. 2008. Disulfide locking a sodium channel voltage sensor reveals ion pair formation during activation. *PNAS* 105:15142–47
45. DeCaen PG, Yarov-Yarovoy V, Sharp EM, Scheuer T, Catterall WA. 2009. Sequential formation of ion pairs during activation of a sodium channel voltage sensor. *PNAS* 106:22498–503
46. DeCaen PG, Yarov-Yarovoy V, Scheuer T, Catterall WA. 2011. Gating charge interactions with the S1 segment during activation of a Na⁺ channel voltage sensor. *PNAS* 108:18825–30
47. Yarov-Yarovoy V, DeCaen PG, Westenbroek RE, Pan CY, Scheuer T, et al. 2012. Structural basis for gating charge movement in the voltage sensor of a sodium channel. *PNAS* 109:E93–102
48. Catterall WA. 1986. Molecular properties of voltage-sensitive sodium channels. *Annu. Rev. Biochem.* 55:953–85
49. Bagneris C, Naylor CE, McCusker EC, Wallace BA. 2015. Structural model of the open-closed-inactivated cycle of prokaryotic voltage-gated sodium channels. *J. Gen. Physiol.* 145:5–16

50. Lenaeus MJ, Gamal El-Din TM, Ing C, Ramanadane K, Pomes R, et al. 2017. Structures of closed and open states of a voltage-gated sodium channel. *PNAS* 114:E3051–60
51. Wisedchaisri G, Tonggu L, McCord E, Gamal El-Din TM, Wang L, et al. 2019. Resting state structure and gating mechanism of a voltage-gated sodium channel. *Cell* 178:993–1003.e12
52. Chakrabarti N, Ing C, Payandeh J, Zheng N, Catterall WA, Pomes R. 2013. Catalysis of Na^+ permeation in the bacterial sodium channel NavAb. *PNAS* 110:11331–36
53. Ulmschneider MB, Bagneris C, McCusker EC, DeCaen PG, Delling M, et al. 2013. Molecular dynamics of ion transport through the open conformation of a bacterial voltage-gated sodium channel. *PNAS* 110:6364–69
54. Naylor CE, Bagneris C, DeCaen PG, Sula A, Scaglione A, et al. 2016. Molecular basis of ion permeability in a voltage-gated sodium channel. *EMBO J.* 35:820–30
55. Heinemann SH, Terlau H, Stühmer W, Imoto K, Numa S. 1992. Calcium channel characteristics conferred on the sodium channel by single mutations. *Nature* 356:441–43
56. Boiteux C, Vorobyov I, Allen TW. 2014. Ion conduction and conformational flexibility of a bacterial voltage-gated sodium channel. *PNAS* 111:3454–59
57. Yue L, Navarro B, Ren D, Ramos A, Clapham DE. 2002. The cation selectivity filter of the bacterial sodium channel, NaChBac. *J. Gen. Physiol.* 120:845–53
58. Tang L, Gamal El-Din TM, Payandeh J, Martinez GQ, Heard TM, et al. 2014. Structural basis for Ca^{2+} selectivity of a voltage-gated calcium channel. *Nature* 505:56–61
59. Hess P, Tsien RW. 1984. Mechanism of ion permeation through calcium channels. *Nature* 309:453–56
60. Almers W, McCleskey EW, Palade PT. 1984. A nonselective cation conductance in frog muscle membrane blocked by micromolar external calcium channels. *J. Physiol.* 353:565–83
61. Sather WA, McCleskey EW. 2003. Permeation and selectivity in calcium channels. *Annu. Rev. Physiol.* 65:133–59
62. Eaton D, Brodwick M, Oxford G, Rudy B. 1978. Arginine-specific reagents remove sodium channel inactivation. *Nature* 271:473–76
63. Pavlov E, Bladen C, Winkfein R, Diao C, Dhaliwal P, French RJ. 2005. The pore, not cytoplasmic domains, underlies inactivation in a prokaryotic sodium channel. *Biophys. J.* 89:232–42
64. Gamal El-Din TM, Martinez GQ, Payandeh J, Scheuer T, Catterall WA. 2013. A gating charge interaction required for late slow inactivation of the bacterial sodium channel NavAb. *J. Gen. Physiol.* 142:181–90
65. Gamal El-Din TM, Lenaeus MJ, Ramanadane K, Zheng N, Catterall WA. 2018. Molecular dissection of multiphase inactivation of the bacterial sodium channel NavAb. *J. Gen. Physiol.* 151:174–85
66. Payandeh J, Gamal El-Din TM, Scheuer T, Zheng N, Catterall WA. 2012. Crystal structure of a voltage-gated sodium channel in two potentially inactivated states. *Nature* 486:135–39
67. Zhang X, Ren W, DeCaen P, Yan C, Tao X, et al. 2012. Crystal structure of an orthologue of the NaChBac voltage-gated sodium channel. *Nature* 486:130–34
68. Zhao Y, Scheuer T, Catterall WA. 2004. Reversed voltage-dependent gating of a bacterial sodium channel with proline substitutions in the S6 transmembrane segment. *PNAS* 101:17873–78
69. Zhao Y, Yarov-Yarovoy V, Scheuer T, Catterall WA. 2004. A gating hinge in Na^+ channels: a molecular switch for electrical signaling. *Neuron* 41:859–65
70. O'Reilly JP, Wang SY, Wang GK. 2001. Residue-specific effects on slow inactivation at V787 in D2-S6 of Nav1.4 sodium channels. *Biophys. J.* 81:2100–11
71. Balsler JR, Nuss HB, Chiamvimonvat N, Pérez-García MT, Marban E, Tomaselli GF. 1996. External pore residue mediates slow inactivation in μ 1 rat skeletal muscle sodium channels. *J. Physiol.* 494:431–42
72. Brown AM, Morimoto K, Tsuda Y, Wilson DL. 1981. Calcium current-dependent and voltage-dependent inactivation of calcium channels in *Helix aspersa*. *J. Physiol.* 320:193–218
73. Kass RS, Sanguinetti MC. 1984. Inactivation of calcium channel current in the calf cardiac Purkinje fiber. Evidence for voltage- and calcium-mediated mechanisms. *J. Gen. Physiol.* 84:705–26
74. Lee KS, Marban E, Tsien RW. 1985. Inactivation of calcium channels in mammalian heart cells: joint dependence on membrane potential and intracellular calcium. *J. Physiol.* 364:395–411

75. Zühlke RD, Pitt GS, Deisseroth K, Tsien RW, Reuter H. 1999. Calmodulin supports both inactivation and facilitation of L-type calcium channels. *Nature* 399:159–62
76. Lee A, Wong ST, Gallagher D, Li B, Storm DR, et al. 1999. Ca²⁺/calmodulin binds to and modulates P/Q-type calcium channels. *Nature* 399:155–59
77. Splawski I, Timothy KW, Sharpe LM, Decher N, Kumar P, et al. 2004. Cav1.2 calcium channel dysfunction causes a multisystem disorder including arrhythmia and autism. *Cell* 119:19–31
78. Splawski I, Timothy KW, Decher N, Kumar P, Sachse FB, et al. 2005. Severe arrhythmia disorder caused by cardiac L-type calcium channel mutations. *PNAS* 102:8089–96
79. Pinggera A, Mackenroth L, Rump A, Schallner J, Beleggia F, et al. 2017. New gain-of-function mutation shows *CACNA1D* as recurrently mutated gene in autism spectrum disorders and epilepsy. *Hum. Mol. Genet.* 26:2923–32
80. Pinggera A, Lieb A, Benedetti B, Lampert M, Monteleone S, et al. 2015. *CACNA1D* de novo mutations in autism spectrum disorders activate Cav1.3 L-type calcium channels. *Biol. Psychiatry* 77:816–22
81. Pinggera A, Negro G, Tuluc P, Brown MJ, Lieb A, Striessnig J. 2018. Gating defects of disease-causing de novo mutations in Cav1.3 Ca²⁺ channels. *Channels* 12:388–402
82. Hondeghem LM, Katzung BG. 1984. Antiarrhythmic agents: the modulated receptor mechanism of action of sodium and calcium channel blocking drugs. *Annu. Rev. Pharmacol. Toxicol.* 24:387–423
83. Kanaya S, Arlock P, Katzung BG, Hondeghem LM. 1983. Diltiazem and verapamil preferentially block inactivated cardiac calcium channels. *J. Mol. Cell. Cardiol.* 15:145–48
84. Khodorov B, Shishkova L, Peganov E, Revenki S. 1976. Inhibition of sodium currents in frog Ranvier node treated with local anesthetics: role of slow sodium inactivation. *Biochim. Biophys. Acta* 433:409–35
85. Hodgkin AL, Huxley AF. 1952. The dual effect of membrane potential on sodium conductance in the giant axon of *Loligo*. *J. Physiol.* 116:497–506
86. Vassilev PM, Scheuer T, Catterall WA. 1988. Identification of an intracellular peptide segment involved in sodium channel inactivation. *Science* 241:1658–61
87. Vassilev P, Scheuer T, Catterall WA. 1989. Inhibition of inactivation of single sodium channels by a site-directed antibody. *PNAS* 86:8147–51
88. Stuhmer W, Conti F, Suzuki H, Wang X, Noda M, et al. 1989. Structural parts involved in activation and inactivation of the sodium channel. *Nature* 339:597–603
89. West JW, Patton DE, Scheuer T, Wang Y, Goldin AL, Catterall WA. 1992. A cluster of hydrophobic amino acid residues required for fast Na⁺ channel inactivation. *PNAS* 89:10910–14
90. Rohl CA, Boeckman FA, Baker C, Scheuer T, Catterall WA, Klevit RE. 1999. Solution structure of the sodium channel inactivation gate. *Biochemistry* 38:855–61
91. McPhee JC, Ragsdale DS, Scheuer T, Catterall WA. 1994. A mutation in segment IVS6 disrupts fast inactivation of sodium channels. *PNAS* 91:12346–50
92. McPhee JC, Ragsdale DS, Scheuer T, Catterall WA. 1995. A critical role for transmembrane segment IVS6 of the sodium channel α subunit in fast inactivation. *J. Biol. Chem.* 270:12025–34
93. McPhee JC, Ragsdale D, Scheuer T, Catterall WA. 1998. A critical role for the S4-S5 intracellular loop in domain IV of the sodium channel α subunit in fast inactivation. *J. Biol. Chem.* 273:1121–29
94. Smith MR, Goldin AL. 1997. Interaction between the sodium channel inactivation linker and domain III S4-S5. *Biophys. J.* 73:1885–95
95. Tang LH, Kallen RG, Horn R. 1996. Role of an S4-S5 linker in sodium channel inactivation probed by mutagenesis and a peptide blocker. *J. Gen. Physiol.* 108:89–104
96. Rogers JC, Qu Y, Tanada TN, Scheuer T, Catterall WA. 1996. Molecular determinants of high affinity binding of α -scorpion toxin and sea anemone toxin in the S3-S4 extracellular loop in domain IV of the Na⁺ channel α subunit. *J. Biol. Chem.* 271:15950–62
97. Sheets MF, Kyle JW, Kallen RG, Hanck DA. 1999. The Na channel voltage sensor associated with inactivation is localized to the external charged residues of domain IV, S4. *Biophys. J.* 77:747–57
98. Chanda B, Bezanilla F. 2002. Tracking voltage-dependent conformational changes in skeletal muscle sodium channel during activation. *J. Gen. Physiol.* 120:629–45

99. Capes DL, Goldschen-Ohm MP, Arcisio-Miranda M, Bezanilla F, Chanda B. 2013. Domain IV voltage-sensor movement is both sufficient and rate limiting for fast inactivation in sodium channels. *J. Gen. Physiol* 142:101–12
100. Hille B. 1977. Local anesthetics: hydrophilic and hydrophobic pathways for the drug-receptor reaction. *J. Gen. Physiol.* 69:497–515
101. Catterall WA. 1987. Common modes of drug action on Na⁺ channels: local anesthetics, antiarrhythmics and anticonvulsants. *Trends Pharmacol. Sci.* 8:57–65
102. Sampson KJ, Kass RK. 2011. Antiarrhythmic drugs. In *Goodman & Gilman's Pharmacological Basis of Therapeutics*, ed. LL Brunton, pp. 815–48. New York: McGraw-Hill. 12th ed.
103. Bean BP. 1984. Nitrendipine block of cardiac calcium channels: high-affinity binding to the inactivated state. *PNAS* 81:6388–92
104. Bean BP, Cohen CJ, Tsien RW. 1983. Lidocaine block of cardiac sodium channels. *J. Gen. Physiol.* 81:613–42
105. Hondeghem LM, Katzung BG. 1977. Timed- and voltage-dependent interactions of antiarrhythmic drugs with cardiac sodium channels. *Biochim. Biophys. Acta* 472:373–98
106. Hille B. 1977. The pH-dependent rate of action of local anesthetics on the node of Ranvier. *J. Gen. Physiol.* 69:475–96
107. Courtney KR. 1980. Structure-activity relations for frequency-dependent sodium channel block in nerve by local anesthetics. *J. Pharmacol. Exp. Ther.* 213:114–19
108. Frazier DT, Narahashi T, Yamada M. 1970. The site of action and active form of local anesthetics. II. Experiments with quaternary compounds. *J. Pharmacol. Exp. Ther.* 171:45–51
109. Narahashi T, Frazier T, Yamada M. 1970. The site of action and active form of local anesthetics. I. Theory and pH experiments with tertiary compounds. *J. Pharmacol. Exp. Ther.* 171:32–44
110. Strichartz GR. 1973. The inhibition of sodium currents in myelinated nerve by quaternary derivatives of lidocaine. *J. Gen. Physiol.* 62:37–57
111. Hille B, Courtney K, Dunn R. 1975. Rate and site of action of local anesthetics in myelinated nerve fibers. In *Molecular Mechanisms of Anesthesia*, Vol. 1: *Progress in Anesthesiology*, ed. BR Fink, pp. 13–20. New York: Raven Press
112. Ragsdale DS, McPhee JC, Scheuer T, Catterall WA. 1994. Molecular determinants of state-dependent block of sodium channels by local anesthetics. *Science* 265:1724–28
113. Ragsdale DS, McPhee JC, Scheuer T, Catterall WA. 1996. Common molecular determinants of local anesthetic, antiarrhythmic, and anticonvulsant block of voltage-gated Na⁺ channels. *PNAS* 93:9270–75
114. Yarov-Yarovoy V, Brown J, Sharp E, Clare JJ, Scheuer T, Catterall WA. 2001. Molecular determinants of voltage-dependent gating and binding of pore-blocking drugs in transmembrane segment III S6 of the Na⁺ channel α subunit. *J. Biol. Chem.* 276:20–27
115. Yarov-Yarovoy V, McPhee JC, Idsvoog D, Pate C, Scheuer T, Catterall WA. 2002. Role of amino acid residues in transmembrane segments IS6 and IIS6 of the sodium channel α subunit in voltage-dependent gating and drug block. *J. Biol. Chem.* 277:35393–401
116. Liu G, Yarov-Yarovoy V, Qu Y, Nobbs M, Clare JJ, et al. 2003. Differential interactions of lamotrigine and related drugs with transmembrane segment IV S6 of voltage-gated sodium channels. *Neuropharmacology* 44:413–22
117. Wang GK, Quan C, Wang S. 1998. A common local anesthetic receptor for benzocaine and etidocaine in voltage-gated mu1 Na⁺ channels. *Pflugers Arch.* 435:293–302
118. Nau C, Wang SY, Wang GK. 2003. Point mutations at L1280 in Nav1.4 channel D3-S6 modulate binding affinity and stereoselectivity of bupivacaine enantiomers. *Mol. Pharmacol.* 63:1398–406
119. Gamal El-Din TM, Lenaeus MJ, Zheng N, Catterall WA. 2018. Fenestrations control resting-state block of a voltage-gated sodium channel. *PNAS* 115:13111–16
120. Glossmann H, Ferry R, Goll A, Striessnig J, Schober M. 1985. Calcium channels: basic properties as revealed by radioligand binding studies. *J. Cardiovasc. Pharmacol.* 7:520–30
121. Gould RJ, Murphy KM, Snyder SH. 1983. Studies on voltage-operated calcium channels using radioligands. *Cold Spring Harb. Symp. Quant. Biol.* 48:355–62

122. Hockerman GH, Peterson BZ, Johnson BD, Catterall WA. 1997. Molecular determinants of drug binding and action on L-type calcium channels. *Annu. Rev. Pharmacol. Toxicol.* 37:361–96
123. Striessnig J, Glossmann H, Catterall WA. 1990. Identification of a phenylalkylamine binding region within the alpha 1 subunit of skeletal muscle Ca²⁺ channels. *PNAS* 87:9108–12
124. Nakayama H, Taki M, Striessnig J, Catterall WA, Kanaoka Y. 1991. Identification of 1,4-dihydropyridine binding regions within the alpha 1 subunit of skeletal muscle Ca²⁺ channels by photoaffinity labeling with diazepam. *PNAS* 88:9203–7
125. Striessnig J, Murphy BJ, Catterall WA. 1991. Dihydropyridine receptor of L-type Ca²⁺ channels: identification of binding domains for [³H](+)-PN200-110 and [³H]azidopine within the alpha 1 subunit. *PNAS* 88:10769–73
126. Catterall WA, Striessnig J. 1992. Receptor sites for Ca²⁺ channel antagonists. *Trends Pharmacol. Sci.* 13:256–62
127. Regulla S, Schneider T, Nastainczyk W, Meyer HE, Hofmann F. 1991. Identification of the site of interaction of the dihydropyridine channel blockers nitrendipine and azidopine with the calcium-channel alpha 1 subunit. *EMBO J.* 10:45–49
128. Schuster A, Lacinová L, Klugbauer N, Ito H, Birnbaumer L, Hofmann F. 1996. The IVS6 segment of the L-type calcium channel is critical for the action of dihydropyridines and phenylalkylamines. *EMBO J.* 15:2365–70
129. Peterson BZ, Catterall WA. 1995. Calcium binding in the pore of L-type calcium channels modulates high affinity dihydropyridine binding. *J. Biol. Chem.* 270:18201–4
130. Peterson BZ, Tanada TN, Catterall WA. 1996. Molecular determinants of high affinity dihydropyridine binding in L-type calcium channels. *J. Biol. Chem.* 271:5293–96
131. Peterson BZ, Hockerman GH, Abbot MR, Johnson BD, Scheuer T, Catterall WA. 1997. Analysis of the dihydropyridine receptor site of L-type calcium channels by alanine-scanning mutagenesis. *J. Biol. Chem.* 272:18752–58
132. Mitterdorfer J, Sinnegger MJ, Grabner M, Striessnig J, Glossmann H. 1995. Coordination of Ca²⁺ by the pore region glutamates is essential for high-affinity dihydropyridine binding to the cardiac Ca²⁺ channel alpha 1 subunit. *Biochemistry* 34:9350–55
133. Mitterdorfer J, Wang ZY, Sinnegger MJ, Hering S, Striessnig J, et al. 1996. Two amino acid residues in the IIIS5 segment of L-type calcium channels differentially contribute to 1,4-dihydropyridine sensitivity. *J. Biol. Chem.* 271:30330–35
134. Hockerman GH, Peterson BZ, Sharp E, Tanada TN, Scheuer T, Catterall WA. 1997. Construction of a high-affinity receptor site for dihydropyridine agonists and antagonists by single amino acid substitutions in a non-L-type Ca²⁺ channel. *PNAS* 94:14906–11
135. Sinnegger MJ, Wang ZY, Grabner M, Hering S, Striessnig J, et al. 1997. Nine L-type amino acid residues confer full 1,4-dihydropyridine sensitivity to the neuronal calcium channel α_{1A} subunit: role of L-type MET¹¹⁸⁸. *J. Biol. Chem.* 272:27686–93
136. Lacinova L, Klugbauer N, Hu M, Hofmann F. 1999. Reconstruction of the dihydropyridine site in a non-L-type calcium channel: the role of the IS6 segment. *FEBS Lett.* 451:152–56
137. Hockerman GH, Johnson BD, Scheuer T, Catterall WA. 1995. Molecular determinants of high affinity phenylalkylamine block of L-type calcium channels. *J. Biol. Chem.* 270:22119–22
138. Hockerman GH, Johnson BD, Abbott MR, Scheuer T, Catterall WA. 1997. Molecular determinants of high affinity phenylalkylamine block of L-type calcium channels in transmembrane segment IIIS6 and the pore region of the α_1 subunit. *J. Biol. Chem.* 272:18759–65
139. Hockerman GH, Dilmac N, Scheuer T, Catterall WA. 2000. Molecular determinants of diltiazem block in domains III S6 and IVS6 of L-type Ca²⁺ channels. *Mol. Pharmacol.* 58:1264–70
140. Johnson BD, Hockerman GH, Scheuer T, Catterall WA. 1996. Distinct effects of mutations in transmembrane segment IVS6 on block of L-type calcium channels by structurally similar phenylalkylamines. *Mol. Pharmacol.* 50:1388–400
141. Brauns T, Cai ZW, Kimball SD, Kang HC, Haugland RP, et al. 1995. Benzothiazepine binding domain of purified L-type calcium channels: direct labeling using a novel fluorescent diltiazem analogue. *Biochemistry* 34:3461–69

142. Kraus R, Reichl B, Kimball SD, Grabner M, Murphy BJ, et al. 1996. Identification of benz(othiazepine)-binding regions within L-type calcium channel $\alpha 1$ subunits. *J. Biol. Chem.* 271:20113–18
143. Tang L, Gamal El-Din TM, Swanson TM, Pryde DC, Scheuer T, et al. 2016. Structural basis for inhibition of a voltage-gated Ca^{2+} channel by Ca^{2+} antagonist drugs. *Nature* 537:117–21
144. Lee KS, Tsien RW. 1983. Mechanism of calcium channel blockade by verapamil, D600, diltiazem, and nitrendipine in single dialysed heart cells. *Nature* 302:790–94
145. Tang L, Gamal El-Din TM, Lenaeus MJ, Zheng N, Catterall WA. 2019. Structural basis for diltiazem block of a voltage-gated Ca^{2+} channel. *Mol. Pharmacol.* 96:485–92
146. Zhao Y, Huang G, Wu J, Wu Q, Gao S, et al. 2019. Molecular basis for ligand modulation of a mammalian voltage-gated Ca^{2+} channel. *Cell* 177:1495–506
147. Davies A, Hendrich J, Van Minh AT, Wratten J, Douglas L, Dolphin AC. 2007. Functional biology of the $\alpha 2\delta$ subunits of voltage-gated calcium channels. *Trends Pharmacol. Sci.* 28:220–28
148. Hoppa MB, Lana B, Margas W, Dolphin AC, Ryan TA. 2012. $\alpha 2\delta$ expression sets presynaptic calcium channel abundance and release probability. *Nature* 486:122–25
149. Hendrich J, Van Minh AT, Hebllich F, Nieto-Rostro M, Watschinger K, et al. 2008. Pharmacological disruption of calcium channel trafficking by the $\alpha 2\delta$ ligand gabapentin. *PNAS* 105:3628–33
150. Bauer CS, Nieto-Rostro M, Rahman W, Tran-Van-Minh A, Ferron L, et al. 2009. The increased trafficking of the calcium channel subunit $\alpha 2\delta-1$ to presynaptic terminals in neuropathic pain is inhibited by the $\alpha 2\delta$ ligand pregabalin. *J. Neurosci.* 29:4076–88
151. Huang W, Liu M, Yan SF, Yan N. 2017. Structure-based assessment of disease-related mutations in human voltage-gated sodium channels. *Protein Cell* 8:401–38
152. Ashcroft FM. 2006. From molecule to malady. *Nature* 440:440–47
153. Jiang D, Gamal El-Din TM, Ing C, Lu P, Pomes R, et al. 2018. Structural basis for gating pore current in periodic paralysis. *Nature* 557:590–94
154. Sokolov S, Scheuer T, Catterall WA. 2010. Ion permeation and block of the gating pore in the voltage sensor of $\text{Nav}1.4$ channels with hypokalemic periodic paralysis mutations. *J. Gen. Physiol.* 136:225–36
155. Ahuja S, Mukund S, Deng L, Khakh K, Chang E, et al. 2015. Structural basis of $\text{Nav}1.7$ inhibition by an isoform-selective small-molecule antagonist. *Science* 350:aac5464
156. Nanou E, Catterall WA. 2018. Calcium channels, synaptic plasticity, and neuropsychiatric disease. *Neuron* 98:466–81



Contents

Introduction to the Theme “Ion Channels and Neuropharmacology: From the Past to the Future” <i>Annette C. Dolphin, Paul A. Insel, Terrence F. Blaschke, and Urs A. Meyer</i>	1
Neurons, Receptors, and Channels <i>David A. Brown</i>	9
Lipid-Dependent Regulation of Ion Channels and G Protein-Coupled Receptors: Insights from Structures and Simulations <i>Anna L. Duncan, Wanling Song, and Mark S.P. Sansom</i>	31
Cryo-Electron Microscopy: Moving Beyond X-Ray Crystal Structures for Drug Receptors and Drug Development <i>Javier García-Nafría and Christopher G. Tate</i>	51
G Protein-Coupled Receptor Pharmacology at the Single-Molecule Level <i>Davide Calebiro and Jak Grimes</i>	73
Structural Basis for Allosteric Modulation of Class B G Protein-Coupled Receptors <i>Denise Wootten and Laurence J. Miller</i>	89
Hyperpolarization-Activated Cyclic Nucleotide-Gated Channels as Drug Targets for Neurological Disorders <i>Bina Santoro and Mala M. Shah</i>	109
Structure and Pharmacology of Voltage-Gated Sodium and Calcium Channels <i>William A. Catterall, Michael J. Linaeus, and Tamer M. Gamal El-Din</i>	133
β_2 Adrenergic Receptor Complexes with the L-type Ca^{2+} Channel $\text{Ca}_v1.2$ and AMPA-Type Glutamate Receptors: Paradigms for Pharmacological Targeting of Protein Interactions <i>Kwun Nok Mimi Man, Manuel F. Navedo, Mary C. Horne, and Johannes W. Hell</i>	155

Targeting the Trafficking of Kidney Water Channels for Therapeutic Benefit <i>Pui W. Cheung, Richard Bouley, and Dennis Brown</i>	175
Levering Mechanically Activated Piezo Channels for Potential Pharmacological Intervention <i>Bailong Xiao</i>	195
Pharmacology of Small- and Intermediate-Conductance Calcium-Activated Potassium Channels <i>Brandon M. Brown, Heesung Shim, Palle Christophersen, and Heike Wulff</i>	219
Neonicotinoid Insecticides: Molecular Targets, Resistance, and Toxicity <i>Kazubiko Matsuda, Makoto Ibara, and David B. Sattelle</i>	241
Neuropathic Pain: Mechanism-Based Therapeutics <i>Kirsty Bannister, Juliane Sachau, Ralf Baron, and Anthony H. Dickenson</i>	257
Barriers to Ensuring Access to Affordable Prescription Drugs <i>Michelle M. Mello</i>	275
Emerging Pharmacological Treatments for Cerebral Edema: Evidence from Clinical Studies <i>Jesse A. Stokum, Volodymyr Gerzanich, Kevin N. Sheth, W. Taylor Kimberly, and J. Marc Simard</i>	291
Gene-Based Dose Optimization in Children <i>Laura B. Ramsey, Jacob T. Brown, Susan I. Vear, Jeffrey R. Bishop, and Sara L. Van Driest</i>	311
Using What We Already Have: Uncovering New Drug Repurposing Strategies in Existing Omics Data <i>Jill M. Pulley, Jillian P. Rhoads, Rebecca N. Jerome, Anup P. Challa, Kevin B. Erreger, Meghan M. Joly, Robert R. Lavieri, Kelly E. Perry, Nicole M. Zaleski, Jana K. Shirey-Rice, and David M. Aronoff</i>	333
Artificial Intelligence in Drug Treatment <i>Eden L. Romm and Igor F. Tsigelny</i>	353
(Inverse) Agonists of Retinoic Acid-Related Orphan Receptor γ : Regulation of Immune Responses, Inflammation, and Autoimmune Disease <i>Anton M. Jetten and Donald N. Cook</i>	371
Engineered Protein Scaffolds as Next-Generation Therapeutics <i>Michaela Gebauer and Arne Skerra</i>	391

The Role of the Microbiome in Drug Response <i>Rosina Pryor, Daniel Martinez-Martinez, Leonor Quintaneiro, and Filipe Cabreiro</i>	417
Prospects for Diminishing the Impact of Nonamyloid Small Vessel Diseases of the Brain <i>Anne Joutel</i>	437
Proteasome Inhibitor Drugs <i>Lloyd D. Fricker</i>	457
Microbiota-Gut-Brain Axis: New Therapeutic Opportunities <i>Caitriona Long-Smith, Kenneth J. O’Riordan, Gerard Clarke, Catherine Stanton, Timothy G. Dinan, and John F. Cryan</i>	477
Drug Therapies for Chronic Cholestatic Liver Diseases <i>Martin Wagner and Peter Fickert</i>	503
Unlocking Personalized Biomedicine and Drug Discovery with Human Induced Pluripotent Stem Cell-Derived Cardiomyocytes: Fit for Purpose or Forever Elusive? <i>Tessa de Korte, Puspita A. Katili, Nurul A.N. Mohd Yusof, Berend J. van Meer, Umber Saleem, Francis L. Burton, Godfrey L. Smith, Peter Clements, Christine L. Mummery, Thomas Eschenbagen, Arne Hansen, and Chris Denning</i>	529
Retinal Pigment Epithelium Replacement Therapy for Age-Related Macular Degeneration: Are We There Yet? <i>Ruchi Sharma, Devika Bose, Arvydas Maminishkis, and Kapil Bharti</i>	553
Big Data and Artificial Intelligence Modeling for Drug Discovery <i>Hao Zhu</i>	573
Device-Based Modulation of Neurocircuits as a Therapeutic for Psychiatric Disorders <i>Zhi-De Deng, Bruce Luber, Nicholas L. Balderston, Melbaliz Velez Afanador, Michelle M. Nob, Jeena Thomas, William C. Altekruse, Shannon L. Exley, Shriya Awasthi, and Sarah H. Lisanby</i>	591
Kappa Opioid Receptor Antagonists as Potential Therapeutics for Stress-Related Disorders <i>Moriah L. Jacobson, Caroline A. Browne, and Irwin Lucki</i>	615
Beyond THC and Endocannabinoids <i>Pal Pacher, Natalya M. Kogan, and Raphael Mechoulam</i>	637
Addressing the Challenge of Polypharmacy <i>Alpana Mair, Martin Wilson, and Tobias Dreischulte</i>	661